

include atomistic modeling of actual FLCs, as was demonstrated earlier for nematics (17). Then the role of explicit chemical substitutions in hypothetical mesogens subjected to  $V(\theta_0)$  and  $V'(R_z)$  can be studied to develop a set of design rules for optimizing spontaneous polarization in FLCs.

## REFERENCES AND NOTES

- R. B. Meyer, presentation at 5th International Liquid Crystal Conference, Stockholm, June 1974; ———, L. Liebert, L. Strzelecki, P. Keller, *J. Phys. Paris Lett.* **36**, 69 (1975); R. B. Meyer, *Mol. Cryst. Liq. Cryst.* **40**, 33 (1977).
- J. W. Goodby, *Science* **231**, 350 (1986).
- R. G. Priest, *J. Chem. Phys.* **65**, 408 (1976); see also W. J. A. Goossens, *Phys. Rev. A* **40**, 4019 (1989).
- D. M. Walba *et al.*, *J. Am. Chem. Soc.* **108**, 5210 (1986).
- J. S. Patel and J. W. Goodby, *Philos. Mag. Lett.* **55**, 283 (1987).
- B. Kutnjak-Urbanc and B. Zeks, *Liq. Cryst.* **18**, 483 (1995).
- Experimental data that could be used to discriminate between dispositions A and B are surprisingly meager [R. Bartolino, J. Doucet, G. Durand, *Ann. Phys. Paris* **3**, 389 (1978); A. Yoshizawa, H. Kikuzaki, M. Fukumasa, *Liq. Cryst.* **18**, 351 (1995)].
- At this minimal level of modeling, the tails are not subject to a direct orientational bias but are biased indirectly through their attachment to the core.
- Here we have chosen to treat  $q^*$  as an external parameter and to approximate the interdependence between  $d_{||}$ ,  $d_{\perp}$ , and  $\alpha$  by the plausible relation  $d_{||} = d_{\perp} \cos \alpha$ , where  $d_{||}$  and  $d_{\perp}$  may be thought of as the respective zone-thickness parameters in the corresponding untitled smectic-A phase.
- We set  $L_{||} = L_{\perp} = L$  and  $\beta_1 = \beta_2 = \beta$  with  $L/L_0 = 0.5$  and  $\beta = 145^\circ$  as representative values in the calculations.
- The tilt  $\tau(T) \propto (T_c - T)^\gamma$ , where  $T_c$  is the smectic-C to smectic-A transition temperature and  $\gamma \leq 0.5$  [P. G. de Gennes and J. Prost, *The Physics of Liquid Crystals* (Oxford Univ. Press, Oxford, ed. 2, 1993), p. 527].
- In a cruder description of orientational averaging in which the stratification constraints are not considered explicitly, each primitive mesogen segment may be thought of as experiencing its own "nematic" orientational potential but with each having a different director orientation. In fact, Priest showed that nonzero polar order parameters are possible using a statistical model of the  $S_C$  phase that contains no first-rank interactions that contribute to the orientational order (3). His model requires that the relevant second-rank tensorial interactions (minimally two) are diagonal in different frames. However, the specification of different principal frames or directors is introduced in an ad hoc way. In order to rationalize the necessity for different frames or directors or to determine their orientations (their respective tilt angles), one has to resort to stratification constraints of the type we use. Moreover, a nonvanishing  $C_{xx}$  can also be obtained even when the tilt angles of the core and the tail segments coincide. An example of this is found in the graphs for  $\alpha \approx 20^\circ$ , for example, the intersection of the dashed curves in Fig. 4B, marked by an arrow.
- J. W. Goodby, *Ferroelectric Liquid Crystals* (Gordon and Breach, Amsterdam, 1991), chap. 2.
- S. Saito *et al.*, *Ferroelectrics* **147**, 367 (1993).
- P. G. de Gennes, *The Physics of Liquid Crystals* (Oxford Univ. Press, Oxford, 2nd printing with additions, 1974), figure 7.18, p. 321; N. A. Clark and S. T. Lagerwall, in (13), chap. 1; figure 8 in (4). Often the polar order of rigid, monoclinic ("zig zag") mesogens in a monoclinic phase is cached in terms of "biased rotation" about the mesogen's long axis, a mechanism that is frequently invoked in phenomenological descriptions of spontaneous polarization (4, 16).
- K. H. Kim, K. Ishikawa, H. Takezoe, A. Fukuda, *Phys. Rev. E* **51**, 2166 (1995).

- D. J. Photinos, E. T. Samulski, H. Toriumi, *J. Chem. Phys.* **94**, 2758 (1991); Z. Luz, D. J. Photinos, E. T. Samulski, *J. Am. Chem. Soc.* **115**, 10895 (1993).
- G. W. Gray and J. W. Goodby, *Mol. Cryst. Liq. Cryst.* **37**, 157 (1976).
- J. W. Goodby, *J. Mater. Chem.* **1**, 307 (1991); ———, I. Nishiyama, A. J. Slaney, C. J. Booth, K. J.

Toyne, *Liq. Cryst.* **14**, 37 (1993).

- This work was supported by National Science Foundation grant DMR-9412701. D.J.P. acknowledges enlightening discussions with N. Clark and M. Glaser.

11 April 1995; accepted 1 August 1995

## Imaging the Electron Density in the Highest Occupied Molecular Orbital of Glycine

Y. Zheng, J. J. Neville, C. E. Brion\*

The spherically averaged electron density distribution of the highest occupied molecular orbital (HOMO) for the amino acid glycine has been determined by multichannel electron momentum spectroscopy. Comparison of the measured HOMO electron momentum distribution with near-Hartree-Fock limit and density functional theory (DFT) calculations for the Boltzmann-weighted sum of the eight predicted stable conformers indicates that electron correlation effects must be included in order to adequately reproduce the experimental results for glycine. The best-fitting DFT calculation determined with the Becke-Perdew gradient-corrected exchange-correlation functional was used to generate HOMO electron density maps for oriented glycine conformers. The result is shown for the most stable conformer.

A detailed knowledge of molecular electron density distribution and electron motion is necessary to improve understanding of molecular recognition and chemical reactivity and to facilitate computer-aided molecular design. To date, molecular modeling procedures rely almost exclusively on total charge distributions obtained from molecular potentials. While detailed information on total charge distributions is available from x-ray and electron scattering experiments, the frontier orbital theory of Fukui (1, 2) predicts that reactivity is influenced primarily by the electron density distribution in the HOMO. Furthermore, it is clear that chemical behavior is influenced predominantly by the valence electrons. It is therefore highly desirable to obtain accurate experimental measurements of valence orbital electron density distributions. Measurements of orbital electron momentum distributions and thus experimental information on orbital electron density can be obtained for atoms and small molecules (3–7) by means of electron momentum spectroscopy (EMS). Recent developments in multichannel EMS (8, 9) have provided the increased sensitivity necessary to study larger molecules of interest in biochemistry and molecular biology. Here, we report EMS measurements and quantum mechanical calculations of the HOMO electron density for the amino acid glycine.

Amino acids are of fundamental biochemical interest because of their role as the basic structural units of proteins. Al-

though there is considerable interest in performing electronic structure calculations on proteins, their large molecular size and structural complexity restrict the level at which conventional theoretical methods [that is, Hartree-Fock (HF) and configuration interaction (CI)] can be used in practice. Less computationally intensive theoretical methods such as DFT (10) hold considerable promise for use with larger biological molecules. It is of key importance to first test such methods on smaller systems, for which EMS measurements can be made and reasonably high level HF calculations of the HOMO electron distribution and other properties are still possible. As the simplest amino acid, glycine not only has a significant role in biological systems but also is an important model compound in biochemistry and therefore an obvious test case for theoretical methods. Although glycine exists as a zwitterion in the solid phase and aqueous solution, in the gas phase it exists as a mixture of neutral conformers (11–13). Recent theoretical (14–19) and experimental (20) studies have considered the number, geometry, and relative energies of these conformers of the glycine molecule.

EMS is an electron impact ionization experiment, in which the kinematics are completely determined by detecting the two outgoing electrons in coincidence (that is, with time correlation) after energy and angle selection (3, 5). The experiment measures spherically averaged electron momentum distributions for individual (binding energy selected) orbitals, that is, orbital imaging in the momentum representation (3, 5, 7). According to the plane wave impulse and the target HF approximations (3, 5, 7), the EMS

Department of Chemistry, University of British Columbia, Vancouver, BC V6T 1Z1, Canada.

\*To whom correspondence should be addressed.

cross section (momentum distribution) is given by

$$\sigma_{\text{EMS}} = \text{constant} \int d\Omega |\psi_i(\mathbf{p})|^2 \quad (1)$$

where  $\mathbf{p}$  is the momentum of the electron before ionization from the target, and the momentum space-independent particle (orbital) wave function  $\psi_i(\mathbf{p})$  is the Fourier transform of the more familiar position space wave function  $\psi_i(\mathbf{r})$ . The quantity  $\int d\Omega$  gives the spherical average over the random orientations of the target molecules. In density functional theory, the target Kohn-Sham approximation (21) results in an expression similar to Eq. 1, but some accounting of electron correlation effects is also included through the exchange-correlation potential. Through use of these theories, EMS measurements have provided a powerful test of

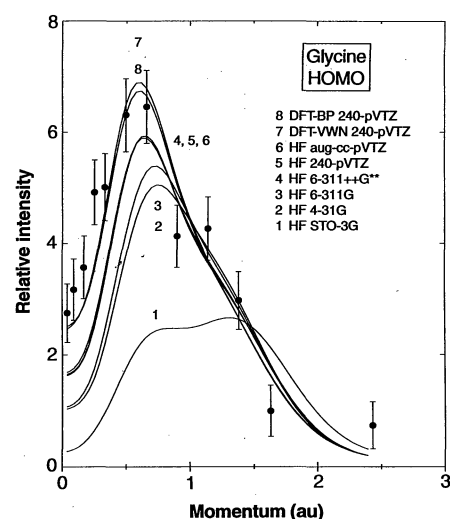


**Fig. 1.** The experimental momentum distribution (●) for the highest occupied molecular orbital of glycine compared with theoretical distributions (curves 1 to 8), which have been obtained with a weighted conformational average. Numbers correspond to the calculations listed in Table 1.

**Table 1.** Calculated and experimental properties for glycine. Hartree-Fock (HF) calculations were done with the program GAUSSIAN92. Density functional theory (DFT) calculations were done with the deMon program (34, 35). Total energies and dipole moments are for the lowest energy (lp) conformer of

Calculation	Method	Basis set	[Heavy atom/H]	Total energy (Hartree)	Dipole moment (Debye)	$\rho_{\text{MAX}}$ (au)
1	HF	STO-3G	[2s, 1p/1s]	-279.114538	1.1850	1.314
2	HF	4-31G	[3s, 2p/2s]	-282.403960	1.2707	0.748
3	HF	6-311G	[4s, 3p/3s]	-282.768248	1.2581	0.723
4	HF	6-311++G**	[5s, 4p, 1d/4s, 1p]	-282.921717	1.2861	0.636
5	HF	240-pVTZ	[5s, 4p, 3d/4s, 3p]	-282.942077	1.2752	0.641
6	HF	aug-cc-pVTZ	[5s, 4p, 3d, 2f/4s, 3p, 2d]	-282.951366	1.2764	0.641
7	DFT-VWN (local)*	240-pVTZ	[5s, 4p, 3d/4s, 3p]	-282.326642	1.2100	0.597
8	DFT-BP (nonlocal)†	240-pVTZ	[5s, 4p, 3d/4s, 3p]	-282.572595	1.1819	0.601
	Experiment				1.0 ± 0.15‡	0.60 ± 0.05

\*The Vosko, Wilk, and Nusair (23) local exchange-correlation potential is used. †The Becke exchange (24) and Perdew correlation (25) gradient corrections to the exchange-correlation potential are used. ‡Suenram and Lovas (12) determined  $\mu_a$  of conformer lp to be  $1.0 \pm 0.15 D$  and  $\mu_b \neq 0$ ,  $\mu_a > \mu_b$ .

ab initio quantum chemical methods (3–5, 7, 8) and have been useful for the evaluation and design of very accurate wave functions (basis sets) for small molecules (4, 5, 22) and for the study of the methyl inductive effect (6). In particular, such studies have shown that electron correlation effects are extremely important in the HOMO orbital densities of small molecules such as water (4, 5) and ammonia (5), but not for hydrocarbons (5). As the application of EMS is extended to problems in biochemistry, it is of key importance to know whether electron correlation effects are important in the valence orbital electron densities of larger molecules such as amino acids. The high sensitivity of EMS experiments to the low-momentum region means that the method is a particularly sensitive probe of the chemically reactive, outer spatial regions of the orbital electron density distribution. These considerations may also have important implications for modeling intramolecular hydrogen bonding in biological molecules (4, 5).

EMS measurements of the HOMO electron momentum distribution of gaseous glycine (Fig. 1) were obtained by means of an energy-dispersive multichannel electron momentum spectrometer with operation conditions as described by Zheng *et al.* (8). The experimental momentum distribution was obtained by recording binding energy spectra at a series of 13 relative azimuthal angles and summing the data at each angle over the binding energy range corresponding to the HOMO, as given by photoelectron spectroscopy (11). The sample was vaporized at 165°C directly into the high-vacuum interaction region of the spectrometer (base pressure,  $10^{-7}$  torr). The experimental results were compared with HF calculations that use a series of basis sets ranging in quality from minimal to near-HF limit, and with large basis set density functional calculations using both local (23) and nonlocal (24, 25) exchange-correlation functionals. The theoretical momentum distributions were obtained through use of the

target HF approximation (5, 7) in the case of the HF calculations and the target Kohn-Sham approximation (21) in the case of the density functional calculations. Calculations were done for each of the eight geometry-optimized conformers predicted by Császár (17) to be minima on the glycine potential energy surface. The study by Császár provides the most complete post-HF survey of possible conformers available and includes a determination of the zero point vibrational energies. Hu *et al.* (18) have recently reported single and double excitation coupled cluster (CCSD) geometry optimization calculations for many of the glycine conformers, and a comparison of their optimized geometries with those reported by Császár for four of the lowest energy conformations (designated Ip, Iip, Iln, and Iip by Császár and I, II, III and IV by Hu *et al.*) shows excellent agreement. For calculation of the momentum distribu-

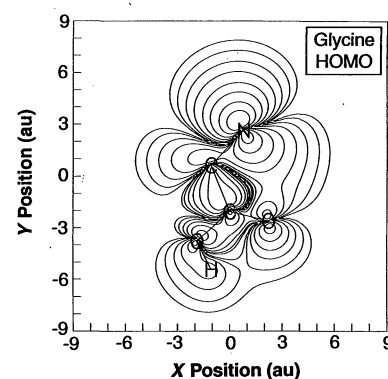


**Fig. 2.** Two-dimensional electron density map for the HOMO of an oriented glycine molecule in the lowest energy conformation (lp), as calculated with the same Kohn-Sham orbital used to obtain momentum distribution 8 in Fig. 1 (see also Table 1). The electron density in the plane of the heavy-atom molecular framework is shown, with the positions of the nuclei comprising this framework indicated by their respective chemical symbols. The contour lines represent 0.01, 0.03, 0.1, 0.3, 1.0, 3.0, 10.0, 30.0, and 99.0% of the maximum density.

glycine (17). Theoretical values of the dipole moment are for a nonrotating, nonvibrating molecule. Calculated  $\rho_{\text{MAX}}$  values are for the Boltzmann-weighted conformer sum so as to correspond with the experimental value. Numbers in the first column correspond to curves 1 to 8 in Fig. 1.

tions, the individual distributions for the eight conformers were summed after being weighted according to the relative Boltzmann populations of the conformers at 165°C, using the relative conformer energies according to the final predictions of Császár together with zero point vibrational energy corrections (17, 26). The weighting factors were 55% (Ip), 20% (IIp), 9% (IIIp), 13% (IVn), 3% (Vn), 0.3% (VIp), 0.1% (VIIp), and 0.1% (VIIIn) where the conformer notation is that used by Császár (17). The individual conformers have significantly different calculated HOMO momentum distributions. The resulting conformer-weighted theoretical momentum distributions (Fig. 1) include folding with the experimental momentum resolution (8) through use of the Gaussian-weighted planar grid (GW-PG) method (27). Details of the various calculations and also the total energies and dipole moments for the most stable conformer (17) and momentum values corresponding to the maximum of the weighted average electron momentum distributions ( $p_{MAX}$ ) are shown in Table 1. The lower level HF treatments with STO-3G, 4-31G, and 6-311G basis sets (curves 1, 2, and 3 in Fig. 1) provide rather poor descriptions of the experimental result. The 6-311++G\*\* basis set, incorporating polarization and diffuse functions, gives an improved HF result (curve 4) similar to that (curve 5) obtained with the 240-pVTZ basis set (28) and to that (curve 6) obtained with the considerably larger aug-cc-pVTZ basis set (29, 30). This result suggests that the HF limit has been quite closely approached with calculations 4, 5, and 6 (see also other properties in Table 1).

Even the better HF calculations (curves 4, 5, and 6 in Fig. 1) seriously underestimate the intensity in the low-momentum region. In contrast, DFT with the 240-pVTZ basis set and either the Vosko, Wilk, and Nusair (VWN) local (23) or the Becke and Perdew (BP) nonlocal gradient-corrected (24, 25) exchange-correlation functional (curves 7 and 8, respectively, in Fig. 1) provides a much improved description of the momentum distribution at lower momentum (<1 atomic unit). This improvement can be attributed to the inclusion of electron correlation effects

via the exchange-correlation potential used in DFT. Figures 2 and 3 show different representations of the position space HOMO electron density map for an oriented glycine molecule for the conformer that is predicted (17) to comprise 55% of the sample at 165°C. These maps were calculated with the nonlocal DFT (240-pVTZ) treatment, which provides the best fit to the experimental momentum distribution (Fig. 1).

Cooper *et al.* (31–33) have recently calculated molecular similarity indices from total electron density distributions in momentum space for possible applications in areas such as drug design (31, 32) and the rationalization of human immunodeficiency virus (HIV) virology data (33). Consideration of the electron density in momentum ( $p$ ) space strongly emphasizes the outermost regions of the valence electron charge density, in contrast to the commonly used position ( $r$ ) space representation, which weights heavily the core (nuclear) region. Using limited basis sets, Cooper *et al.* (33) have shown that there is a high degree of correspondence between the half-maximal effective dose (ED<sub>50</sub>) clinical activity of anti-HIV phospholipids and theoretical predictions when the densities are considered in momentum space. This result can be attributed to the extremely high sensitivity of the momentum space representation to the chemically sensitive outer spatial (larger  $r$ ) regions of the charge distribution, which are of key importance in molecular recognition. In other studies of structure-reactivity relations in the context of drug design (31) and molecular similarity studies (32), Cooper and Allan suggest that it would be interesting and potentially fruitful if momentum space calculations were done on a HOMO/LUMO orbital rather than a total density basis. Electron momentum spectroscopy provides such orbital density information directly in momentum space, and our experimental results and related theoretical investigations for glycine show that details of the HOMO electron density distributions can be obtained for biologically important molecules. In particular, the need to include electron correlation effects in describing the reactive part of the

electron distribution of the amino acid glycine has been demonstrated by comparison of EMS measurements with density functional theory calculations for the contributing conformers.

## REFERENCES AND NOTES

1. K. Fukui, in *Proceedings of the Nobel Laureate Symposium on Applied Quantum Chemistry*, V. H. Smith Jr., H. F. Schaefer III, K. Morokuma, Eds. (Reidel, Boston, 1986), pp. 1–25.
2. ———, T. Yonezawa, H. J. Shingu, *J. Chem. Phys.* **20**, 722 (1952).
3. C. E. Brion, *Int. J. Quantum Chem.* **29**, 1397 (1986).
4. A. O. Bawagan, C. E. Brion, E. R. Davidson, D. Feller, *Chem. Phys.* **113**, 19 (1987).
5. C. E. Brion, in *The Physics of Electronic and Atomic Collisions*, T. Andersen *et al.*, Eds. (American Institute of Physics, New York, 1993), pp. 350–359.
6. A. O. Bawagan and C. E. Brion, *Chem. Phys. Lett.* **137**, 573 (1987); *Chem. Phys.* **123**, 51 (1988).
7. I. McCarthy and E. Weigold, *Rep. Prog. Phys.* **91**, 789 (1991).
8. Y. Zheng *et al.*, *Chem. Phys.* **188**, 109 (1994).
9. B. R. Todd, N. Lerner, C. E. Brion, *Rev. Sci. Instrum.* **65**, 349 (1994).
10. R. G. Parr and W. Yang, *Density Functional Theory of Atoms and Molecules* (Oxford Univ. Press, New York, 1989).
11. T. P. Debies and J. W. Rabalais, *J. Electron Spectrosc. Relat. Phenom.* **3**, 315 (1974).
12. R. D. Suenram and F. J. Lovas, *J. Am. Chem. Soc.* **102**, 7180 (1980).
13. K. Iijima *et al.*, *J. Mol. Struct.* **246**, 257 (1991).
14. J. H. Jensen and M. S. Gordon, *J. Am. Chem. Soc.* **113**, 7917 (1991).
15. M. Ramek *et al.*, *J. Mol. Struct.* **235**, 1 (1991).
16. R. F. Frey *et al.*, *J. Am. Chem. Soc.* **114**, 5369 (1992).
17. A. G. Császár, *ibid.*, p. 9568.
18. C.-H. Hu *et al.*, *ibid.* **115**, 2923 (1993).
19. V. Barone *et al.*, *J. Chem. Phys.* **102**, 364 (1995).
20. P. D. Godfrey and R. D. Brown, *J. Am. Chem. Soc.* **117**, 2019 (1995).
21. P. Duffy *et al.*, *Phys. Rev. A* **50**, 4707 (1994).
22. D. Feller, C. M. Boyle, E. R. Davidson, *J. Chem. Phys.* **86**, 3424 (1987).
23. S. H. Vosko, L. Wilk, M. Nusair, *Can. J. Phys.* **58**, 1200 (1980).
24. A. D. Becke, *Phys. Rev. A* **38**, 3098 (1988).
25. J. P. Perdew, *Phys. Rev. B* **33**, 8822 (1986).
26. D. Yu *et al.*, *Can. J. Chem.* **70**, 1762 (1992).
27. P. Duffy *et al.*, *Chem. Phys.* **159**, 347 (1992).
28. The 240-pVTZ basis set is the aug-cc-pVTZ basis set of Dunning *et al.* (29, 30), with the  $f$  functions on the heavy atoms and the  $d$  functions on the hydrogens removed. This truncation was done because the existing version of the deMon DFT program cannot process  $f$  functions. The truncation produces very little change in the calculated momentum distribution (compare curves 5 and 6 in Fig. 1) and only small differences in the total energy and dipole moment (see Table 1).
29. T. H. Dunning Jr., *J. Chem. Phys.* **90**, 1007 (1989).
30. R. A. Kendall *et al.*, *ibid.* **96**, 6796 (1992).
31. D. L. Cooper and N. L. Allan, *J. Comput. Aided Mol. Des.* **3**, 253 (1989).
32. ———, *J. Am. Chem. Soc.* **114**, 4773 (1992).
33. D. L. Cooper *et al.*, *ibid.* **115**, 12615 (1993).
34. A. St-Amant and D. R. Salahub, *Chem. Phys. Lett.* **169**, 387 (1990).
35. D. R. Salahub *et al.*, in *Density Functional Methods in Chemistry*, J. Labanowski and J. Andzelm, Eds. (Springer-Verlag, New York, 1991), pp. 77–100.
36. Support by the Canadian National Networks of Centres of Excellence Program—Centre of Excellence in Molecular and Interfacial Dynamics (CEMAID) and the Natural Sciences and Engineering Research Council of Canada (NSERC). J.J.N. gratefully acknowledges the receipt of an NSERC postgraduate scholarship. We thank A. O. Bawagan for helpful discussions.

**Fig. 3.** A three-dimensional representation of the electron density in the molecular plane of the HOMO of an oriented molecule in the lowest energy conformation (Ip) of gaseous glycine, as calculated with the same Kohn-Sham orbital used to obtain momentum distribution 8 in Fig. 1 (see also Table 1). Note that the (vertical) relative electron density scale is linear.

